Saudi Journal of Biological Sciences 29 (2022) 1029–1042

Contents lists available at ScienceDirect

Saudi Journal of Biological Sciences

journal homepage: www.sciencedirect.com

Original article

# Alpha-glucosidase inhibitors from *Nervilia concolor*, *Tecoma stans*, and *Bouea macrophylla*

Kim-Ngoc Ha [a], Tran-Van-Anh Nguyen [b], Dinh-Tri Mai [c,d], Nguyen-Minh-An Tran [e], Ngoc-Hong Nguyen [a], Giau Van Vo [f,g], Thuc-Huy Duong [h,*], Huy Truong Nguyen [b,*]

[a] *CirTech Institute, Ho Chi Minh City University of Technology (HUTECH), 475 A Dien Bien Phu Street, Binh Thanh District, Ho Chi Minh City 700000, Viet Nam*
[b] *Faculty of Pharmacy, Ton Duc Thang University, Ho Chi Minh City 700000, Viet Nam*
[c] *Graduate University of Science and Technology, Vietnam Academy of Science and Technology, 18 Hoang Quoc Viet, Cau Giay, Ha Noi 11355, Viet Nam*
[d] *Institute of Chemical Technology, Vietnam Academy of Science and Technology, 01 Mac Dinh Chi, Ho Chi Minh City 71007, Viet Nam*
[e] *Faculty of Chemical Engineering, Industrial University of Ho Chi Minh City, Ho Chi Minh City 71420, Viet Nam*
[f] *Department of Biomedical Engineering, School of Medicine, Vietnam National University – Ho Chi Minh City (VNU-HCM), Ho Chi Minh City, Viet Nam*
[g] *Vietnam National University – Ho Chi Minh City (VNU-HCM), Ho Chi Minh City 700000, Viet Nam*
[h] *Department of Chemistry, University of Education, 280 An Duong Vuong Street, District 5, Ho Chi Minh City 72711, Viet Nam*

ARTICLE INFO

*Article history:*
Received 25 July 2021
Revised 18 September 2021
Accepted 25 September 2021
Available online 30 September 2021

*Keyword:*
*Tecoma stans*
*Nervilia concolor*
*Bouea macrophylla*
Ursolic acid
Alpha-glucosidase
Flavonoids
Molecular docking
Molecular dynamic simulations

ABSTRACT

*Tecoma stans* (L.) Juss. Ex Kunth is widely used in folk medicine. In ethnomedicine, it is applied as a cardioprotective, hepatoprotective, antiarthritic, antinociceptive, anti-inflammatory, and antimicrobial. The aqueous extract is considered antidiabetic, and is used as a traditional remedy in Mexico. More than 120 chemical constituents have been identified in its leaves, barks, and roots. However, less is known about the phytochemical properties of *T. stans* flower extracts. The herbal plant *Nervilia concolor* (Blume) Schltr. is native to Vietnam, and is used in traditional Chinese medicine to treat diseases such as bronchitis, stomatitis, acute pneumonia, and laryngitis. Only two previous reports have addressed the chemical content of this plant. *Bouea macrophylla* Griff., commonly known as marian plum or plum mango, is a tropical plant that is used to treat a range of illnesses. Phytochemical analysis of *B. macrophylla* suggests the presence of volatile components and flavonoids. However, existing data have been obtained from screening without isolation. As part of our ongoing search for alpha-glucosidase inhibitors from Vietnamese medicinal plants, we conducted bioactive-guided isolation of the whole plant *N. concolor,* the flowers of *T. stans,* and the leaves of *B. macrophylla*. We isolated and structurally elucidated five known compounds from *T. stans*: ursolic acid (**TS1**), 3-oxours-12-en-28-oic acid (**TS2**), chrysoeriol (**TS3**), ferulic acid (**TS4**), and tecomine (**TS5**). Three known compounds were isolated from *Nervilia concolor*: astragalin (**NC1**), isoquercitrin (**NC2**), and caffeic acid (**NC3**). From *B. macrophylla*, betullinic acid (**BM1**), methyl gallate (**BM2**), and 3-*O*-galloyl gallic acid methyl ester (**BM3**) were isolated. All compounds showed promising alpha-glucosidase inhibition, with $IC_{50}$ values ranging from 1.4 to 143.3 μM. The kinetics of enzyme inhibition showed **BM3** to be a competitive-type inhibitor. An *in silico* molecular docking model confirmed that compounds **NC1**, **NC2,** and **BM3** were potential inhibitors of the α-glucosidase enzyme. Molecular dynamics simulations were carried out with compound **BM3** demonstrating the best docking model during simulation up to 100 ns to explore the stability of the complex ligand–protein.


## 1. Introduction

*Tecoma stans (L.) Juss. Ex Kunth* (common names: yellow-elder or yellow-bell) is a globally-used folk medicine. In Mexico, it has been used to treat diabetes. Comprehensive reviews have identified its use as a hypoglycemic, cardioprotective, cytotoxic, anticancer, hepatoprotective, antimicrobial, antinociceptive, anti-inflammatory, antiarthritic, antispasmodic, antiadiarrrheal, and antiulcer agent (Anand and Basavaraju, 2020; Raju et al., 2011a, b; Kumar and Boopathi, 2018; Dohnal, 1977). The aqueous extract

* Corresponding authors at: Department of Chemistry, Ho Chi Minh City University of Education, 280 An Duong Vuong Street, District 5, 748342 Ho Chi Minh City, Viet Nam (T.-H. Duong). Faculty of Pharmacy, Ton Duc Thang University, Ho Chi Minh City 700000, Viet Nam (H. T. Nguyen).
*E-mail addresses:* huydt@hcmue.edu.vn (T.-H. Duong), nguyentruonghuy@tdtu.edu.vn (H. Truong Nguyen).
Peer review under responsibility of King Saud University.

Production and hosting by Elsevier

https://doi.org/10.1016/j.sjbs.2021.09.070
1319-562X/

shows significant antidiabetic properties, reflecting its traditional uses (Taher et al., 2016; Aguilar-Santamaría et al., 2009). Phytochemical analyses of *Tecoma stans* have isolated over 120 compounds with a diversity of skeletons. They include monoterpene alkaloids, flavonoids, terpenoids, glycosides, and volatile components. All parts of the plant have been chemically analysed (Anand and Basavaraju, 2020), though little is understood about the chemistry of the flowers. Earlier studies have reported two carotenoids and four glycosides from floral extracts (Anand and Basavaraju, 2020). The crude extracts have been evaluated for antioxidant, anti-proliferative (Marzouk et al., 2006), nephrotoxic (Raju et al., 2011a,b), hepatoprotective (Kameshwara et al., 2013), and antimicrobial (Costantino et al., 2003) properties.

The herbal plant *Nervilia concolor* (Blume) Schltr. (Orchidaceae) (syn. *N. aragoana*) is native to Vietnam, and is widely distributed in high-altitude areas. It is used in traditional Chinese medicine to treat a variety of conditions including bronchitis, stomatitis, acute pneumonia, and laryngitis (Gale et al., 2007; Chen et al., 2013; Qiu et al., 2013; Tian et al., 2009; Zhou et al., 2009; Zhang et al., 2012). Previous studies of the native Vietnamese species *N. concolor* (syn. *N. aragoana*) have reported two new cycloartane glycosides, 12 flavonoids, and one novel compound (Tran et al., 2019a, 2019b).

*Bouea macrophylla* Griff., commonly known as marian plum or plum mango, is a medicinal plant that grows in tropical regions (Thummajitsakul and Silprasit, 2017), including South East Asia. It is used as a folk medicine for the treatment of a range of illnesses (Nguyen et al., 2020). The ethanol extracted from its leaves has been used as an adjuvant for cancer treatment in South Kalimantan (Dechsupa et al., 2019; Fitri et al., 2018). However, few phytochemical data are available, and those that exist rely mainly on screening without isolation (Nguyen et al., 2020; Dechsupa et al., 2019; Fitri et al., 2018; Sukalingam 2018). The methanolic extract from the leaves provides a rich source of alkaloids, anthraquinones, triterpenoids, saponins, flavonoids, phenolic compounds, and vitamin C (Rajan and Bhat, 2016). HPLC and LC/MS analyses have identified pentagalloyl glucose (PGG), ethyl gallate, and gallic acid in the hydroethanolic extracts from *B. macrophylla* seeds (Dechsupa et al., 2019). A recent study of the ethanolic extract using GC–MS methods reported the isolation of 14 volatile compounds (Nguyen et al., 2020).

While accessible sources of *Tecoma stans* have been phytochemically investigated, little is known about the chemical profiles of *N. concolor* and *B. macrophylla*. In particular, no previous studies have investigated alpha-glucosidase inhibition by extracts from *N. concolor,* the flowers of *T. stans,* or the leaves of *B. macrophylla*. In this paper, we report the bioactive-guided isolation of such extracts. The chemical structures of eleven known compounds (TS1-5, NC1-3, BM1-3) were elucidated using spectroscopic data, and the results compared with those available in the literature (Fig. 1). The isolated compounds were evaluated for alpha-glucosidase inhibition and molecular docking studies were performed to elucidate the mechanisms involved.

## 2. Experimental

### 2.1. General experimental procedures

NMR spectra were recorded on a Bruker Avance III spectrometer (500 MHz for $^{1}$H NMR and 125 MHz for $^{13}$C NMR) using residual solvent signals as internal references: acetone $d_6$ at $\delta_H$ 2.05, $\delta_C$ 29.84 and chloroform-*d* at $\delta_H$ 7.26, $\delta_C$ 77.18. Thin layer chromatography (TLC) was carried out on precoated silica gel 60 $F_{254}$ or silica gel 60 RP–18 $F_{254S}$ (Merck), and spots were visualized by spraying with 10% $H_2SO_4$ solution followed by heating. Gravity column chromatography was performed on silica gel 60 (0.040–0.063 mm, Himedia).

### 2.2. Source of plant material

Whole *N. condolor* plants were collected in Cu M'gar district, Dak Lak province, in August 2020 and identified by Assoc. Prof. Dr. Tran Hop, Institute of Tropical Biology, Vietnam Academy of Science and Technology, Ho Chi Minh City, Vietnam. A voucher specimen (No. NA-0621) was deposited with the Bioactive Compounds Laboratory, Institute of Chemical Technology.

Leaves of *B. macrophylla* were collected in Vinh Long Province, Vietnam in May 2020. The scientific name of the plant was authenticated by Dr. Tran Cong Luan, Tay Do University. A voucher specimen (No. UP019) was deposited with the Department of Chemistry, Ho Chi Minh University of Education.

Flowers of T. stans were collected in Ho Chi Minh City, Vietnam between April and June 2020. The scientific name of the plant was authenticated by Dr. Tran Cong Luan, Tay Do University. A voucher specimen (No. UP020) was deposited with the Department of Chemistry, Ho Chi Minh University of Education.

### 2.3. Alpha-glucosidase inhibition assay

Saccharomyces cerevisiae α-glucosidase (E.C 3.2.1.20), acarbose, and 4-nitrophenyl β-D-glucopyranoside (pNPG) were obtained from Sigma-Aldrich Co (Saint Louis, MI, USA). The alpha-glucosidase (0.2 U/mL) and substrate (5.0 mM p-nitrophenyl-β -D-glucopyranoside) were dissolved in 100 mM of pH 6.9 sodium phosphate buffer (Devi et al., 2020). The inhibitor (50 μL) was preincubated with alpha-glucosidase at 37 °C for 20 min, then 40 μL of substrate was added to the reaction mixture. The enzymatic reaction was carried out at 37 °C for 20 min and stopped by adding 0.2 M $Na_2CO_3$ (130 μL). The method followed that in a previous report (Devi et al., 2020).

### 2.4. Inhibitory type assay of BM3 on alpha-glucosidase

The mechanism of alpha-glucosidase inhibition by BM3 was determined using Lineweaver-Burk plots (Microsoft Excel 2010, Washington, USA), following methods reported in the literature (Tran et al., 2021). Enzyme inhibition at the different BM3 concentrations was evaluated from the substrate. Using Lineweaver–Burk double reciprocal plots 1/enzyme velocity (1/V) vs. 1/substrate concentration (1/[S]), the inhibition type was determined at *p*NPG substrate concentrations of 1 mM, 2 mM, and 4 mM in the presence of test compound concentrations of 0, 9.3, 18.6, and 37.2 μM. Three replications were used. The mixtures were incubated at 37 °C and the optical density was measured at 405 nm over 30 min, at intervals of 1 min, using a Clariostar Labtech microplate reader (Ortenberg, Germany). $IC_{50}$ values were used to identify the optimal test compound concentrations. The inhibition constants were obtained graphically from secondary plots (Microsoft Excel 2010, Washington, USA).

### 2.5. Molecular docking study

The calculations performed in the molecular docking model, which was based on previous article (Duong et al., 2020). The docking steps performed in Scheme 1 by AutoDockTools-1.5.6rc3 package. The docking parameters set up in grid logic file (dock.gpf) with the values of grid point spacing, user-specified grid points, and coordinates of central grid Point of maps, which installed 0.608 Angstroms, (126, 100, 124 points), and (6.403, 0.143, 9.743), respectively. One receptor was the crystal structures of enzyme α-glucosidase enzyme, which has code 4J5T (code: 4J5T). It has collected from protein data bank. The ligands have been used for docking was NC1, NC2, BM3, and Acarbose (standard drug). Before making docking, the ligand has conducted the optimal

conformation by MMFF94 method by Avogadro software and saved as by file name of ligand.pdb. For receptor, 4J5T, it was deleted the water molecules, the small ligands, and the heteroatom atoms, which were available in co-crystal structure. Finally, it was saved as by a file name of receptor, receptor.pdb. The validation of docking or redocking method has followed the article (Sibanyoni et al., 2020). After completing of docking calculation, the best stable conformation ligand of one ligand was selected and docked to crystal structure of an enzyme α-glucose, 4J5T, which was target enzyme or receptor.

### 2.6. Molecular dynamics simulation

Molecular dynamics (MD) were simulated on the docked complex BM3-4J5T by using GROMACS program with Amber99SB-IDLN (Lindorff-Larsen et al., 2010). Antechamber software was adopted to construct the topology and general Amber force field parameters for ligand BM3, and those parameters were converted by ACPYPE python script (Sousa da Silva and Vranken, 2012) to make them readable on GROMACS. Later, TIP3P water molecules (Jorgensen et al., 1983) were embedded into the system and a dodecahedron periodic boundary condition box. Then, the whole system was neutralized with the water removal and sodium ions addition. The neutral solvated system was firstly minimized of energy with 50,000 steps of steepest integrator, secondly equilibrated in 100 ps of NVT ensembles (T = 300 K) and 100 ps of NPT ensembles (T = 300 K, P = 1 atm). The MD simulations were lastly performed with 100 ns of an integrator with a time interval of 2 fs. Two independent trajectories were executed for further analysis.

Those emerging trajectories were analyzed by embedded modules of GROMACS for root-mean-square deviation (RMSD), root mean square fluctuations (RMSF) on the C-alpha residue; radius of gyration ($R_g$); solvent accessible surface area (SASA), and the hydrogen bond by *gmx rms*, *gmx rmsf*, *gmx gyrate*, *gmx sasa*, and *gmx hbond* respectively. Then the graphs were extracted using XMGRACE software. Additional RMSD value was also calculated between reference structure and MD-refined structure obtained by clustering method with 1.5 Å cut-off over equilibrium interval of 50–60 ns.

The molecular mechanics/Poisson-Boltzmann surface area (MM/PBSA) method was applied to estimate the binding free energy based on previous MD studies (Ngo et al., 2021; Poli et al., 2020). The free energies calculated over 50 frames of an interval of 50–100 ns were obtained from the following sum:

$$\Delta E_{elec} + \Delta E_{vdW} + \Delta G_{polar} + \Delta G_{sa}$$

where the two first terms are electrostatic and van der Waals interactions (Al-Shabib et al., 2020) in gas phase, the two last terms are the free energy for polar and apolar solvations. Herein, the nonpolar solvation energy is modeled on the relation to solvent accessible surface area (SASA).

### 2.7. Extraction and isolation

#### 2.7.1. Isolation of Tecoma stans

Dried *T. stans* (5.2 kg) flowers were crushed and extracted for 24 h with MeOH (3 × 20 L) at ambient temperature. The filtrated solution was evaporated to dryness under reduced pressure to obtain a crude extract (315 g). This was successively partitioned by *n*-hexane, *n*-hexane: EtOAc (1:1, v/v), and EtOAc to afford extracts H (28 g), HEA (67 g), and EA (88.0 g). Fraction HEA (67 g) was subjected to silica gel column chromatography (CC), using an isocratic mobile phase consisting of *n*-hexane: EtOAc: acetone (8:1:1, v/v/v) to obtain fractions HEA1 (5.3 g), HEA2 (11.4 g), HEA3 (21.2 g), HEA4 (6.9 g), and HEA5 (14.8 g). Fraction HEA4 (6.9 g) was dissolved in methanol to obtain HEA4T as a solid and HEA4S in solution. The HEA4T (1.3 g) was subjected to silica gel column chromatography, using a solvent system of *n*-hexane: $CHCl_3$: EtOAc: acetone (10:6:2:1, v/v/v/v), yielding compounds TS1 (620 mg) and TS2 (4.9 mg). The HEA4S (5.4 g) was subjected to Sephadex LH-20 gel chromatography, eluted with methanol, to obtain fractions S1-4. Fraction S1.3 (2.9 g) was subjected to silica gel CC using a solvent system of *n*-hexane: $CHCl_3$: methanol (5:6:0.5,v/v/v/v), affording fractions S1.3.1- S1.3.8. Fraction S1.3.3 (201 mg) was fractionated by silica gel CC using the same solvent system, affording compound TS4 (2.1 mg). Fraction S1.3.7 (101 mg) was subjected to C-18 reverse-phase silica gel CC eluted with MeOH: $H_2O$ (2 :1, v/v), yielding compounds TS3 (7.9 mg) and TS5 (2.1 mg).

#### 2.7.2. Isolation of Nervilia condolor

Whole *N. condolor* (4.1 kg) plant was powdered then extracted three times (3 × 30 L) with 96% EtOH at room temperature. Solvents were removed under low pressure to provide a crude extract (281 g). The residue was dried then successively re-extracted using solvents of increasing polarity: *n*-hexane (H, 110 g), $CHCl_3$ (C, 30 g), and EtOAc (EA, 91 g). The extract EA (91 g) was subjected to silica gel column chromatography and eluted with a gradient of chloroform–methanol (50:1 → 0:10 %) to afford fractions EA1 (14.5 g), EA2 (27 g), EA3 (21 g), EA4 (15 g), and EA5 (8.5 g). Fraction EA5 (8.5 g) was chromatographed over silica gel CC, eluting with CHCl3-MeOH (15:1, v/v), to obtain fractions EA5.1-6. Fraction EA5.2 (1.5 g) was rechromatographed by silica gel CC, eluted with $CHCl_3$: MeOH: $H_2O$ (10:1:0.1, v/v/v), to yield compound NC3 (31 mg). Fraction EA5.5 (2.1 g) was subjected to silica gel CC, eluted with $CHCl_3$: MeOH: $H_2O$ (7:1:0.1, v/v/v), to yield compounds NC1 (17 mg) and NC2 (14 mg).

#### 2.7.3. Isolation of Bouea macrophylla

Fresh *B. macrophylla* leaves (47 kg) were washed under running tap water and air-dried. The ground powder (20 kg) was macerated with MeOH (3 × 30 L) at room temperature. After filtration, the solvent was evaporated to dryness under reduced pressure, yielding the crude MeOH residue (792 g). This was subjected to liquid–liquid extraction using solvents of *n*-hexane, *n*-hexane-EtOAc (1:1, v/v) and EtOAc to yield *n*-hexane (H, 214 g), *n*-hexane-EtOAc (HEA, 30.6 g), and EtOAc (EA, 390 g) extracts. The HEA was loaded onto Sephadex LH-20 CC and eluted with MeOH to give fractions HEA1-5. HEA3 (7.6 g) was washed with methanol (5x100 mL). The resulting solid was crystallized in acetone to obtain compound BM1 (1.3 g). Fraction HEA4 (6.2 g) was rechromatographed using Sephadex LH-20 CC, providing fractions HEA4.1-4.4. The HEA4.3 (1.9 g) was subjected to silica gel CC and eluted with a solvent system of *n*-hexane-EtOAc (2:1, v/v) to obtain sub-fractions HEA431-435. The HEA434 (101 mg) was subjected to silica gel column chromatography and eluted with a solvent system of *n*-hexane-EtOAc (1:1, v/v) to give BM2 (210 mg) and BM3 (5 mg).

## 3. Results

Extracts/fractions from *N. concolor*, *T. stans*, and *B. macrophylla* were evaluated for alpha-glucosidase inhibition (Table 1). The most active extract of each plant was selected for further isolation.

### 3.1. Phytochemical identification and alpha-glucosidase inhibition of isolated compounds of Tecoma stans

From *Tecoma stans*, five known compounds were isolated from the bioactive fraction HEA4 of *T. stans:* ursolic acid (TS1), 3-oxours-12-en-28-oic acid (TS2), chrysoeriol (TS3), ferulic acid

**Table 1**
Alpha-glucosidase inhibition ($IC_{50}$) by extracts and fractions.

| Bio-source | Extracts | $IC_{50}$ μg/mL |
|---|---|---|
| ***Tecoma stans*** | Crude MeOH | 205.7 |
| | *n*-Hexane (Extract **H**) | >200 |
| | *n*-Hexane: ethyl acetate (Extract **HEA**) | 89.8 |
| | Ethyl acetate (Extract **EA**) | >200 |
| | Fraction **HEA1** | >200 |
| | Fraction **HEA2** | >200 |
| | Fraction **HEA3** | 137.2 |
| | Fraction **HEA4** | 87.8 |
| | Fraction **HEA5** | >200 |
| ***Nervilia concolor*** | Crude EtOH | 79.9 |
| | *n*-Hexane (Extract **H**) | 37.6 |
| | Chlroform (Extract **C**) | 35.4 |
| | Ethyl acetate (Extract **EA**) | 18.4 |
| ***Bouea macrophylla*** | Crude MeOH | 185.4 |
| | *n*-Hexane (Extract **H**) | >200 |
| | *n*-Hexane: ethyl acetate (Extract **HEA**) | 98.3 |
| | Ethyl acetate (Extract **EA**) | >200 |
| | Fraction **HEA1** | >200 |
| | Fraction **HEA2** | >200 |
| | Fraction **HEA3** | 78.8 |
| | Fraction **HEA4** | 96.4 |
| | Fraction **HEA5** | >200 |

(TS4), and tecomine (TS5). The compounds were readily identified from their 1D- and 2D-NMR spectra (Table S1, Fig. S1-5). All isolated compounds were the first to be reported from the studied plant.

Ursolic acid (TS1). White amorphous powder. $^1$H NMR (500 MHz, Acetone $d_6$) and $^{13}$C NMR (125 MHz, Acetone $d_6$) data were consistent with those reported in the literature (Basir et al., 2014).

3-Oxours-12-en-28-oic acid (TS2). White amorphous powder. $^1$H NMR (500 MHz, Acetone $d_6$) data were consistent with those reported in the literature (Basir et al., 2014).

Chrysoeriol (TS3). Light yellow amorphous powder. $^1$H NMR (500 MHz, DMSO $d_6$) and $^{13}$C NMR (125 MHz, DMSO $d_6$) data were consistent with those reported in the literature (Bashyal et al., 2019). See Table S2, Fig. S8.

Ferulic acid (TS4). White amorphous powder. $^1$H NMR (500 MHz, Acetone $d_6$) data were consistent with those reported in the literature (Shimomura et al., 1988).

Tecomine (TS5). White amorphous powder. $^1$H NMR (500 MHz, Acetone $d_6$) data were consistent with those reported in the literature (Lins and Felicio, 1993) (Fig. S9).

The isolated compounds TS1-5 were evaluated the alpha-glucosidase inhibition. All exhibited potent inhibition of alpha-glucosidase with $IC_{50}$ values ranging from 39.2 to 143.3 μM. This exceeded the $IC_{50}$ 332.5 μM of the acarbose standard (Table 2).

### 3.2. Phytochemical identification and alpha-glucosidase inhibition of isolated compounds of Nervilia concolor

From *Nervilia concolor*, three known compounds were isolated: astragalin (NC1), isoquercitrin (NC2), and caffeic acid (NC3) from the active extract EA.

Astragalin (NC1). Yellow amorphous powder. $^1$H NMR (500 MHz, DMSO $d_6$) and $^{13}$C NMR (125 MHz, DMSO $d_6$) data were consistent with those reported in the literature (Rezende et al., 2019). See Table S2, Fig. S10.

Isoquercitrin (NC2). Yellow amorphous powder. $^1$H NMR (500 MHz, DMSO $d_6$) and $^{13}$C NMR (125 MHz, DMSO $d_6$) data were consistent with those reported in the literature (Napolitano et al., 2012). See Table S2, Fig. S11.

**Table 2**
Alpha-glucosidase inhibition ($IC_{50}$) by compounds **NC1-3, TS1-5,** and **BM1-3.**

| Compounds | $IC_{50}$ μM |
|---|---|
| **TS1** | 39.2 ± 0.6 |
| **TS2** | 82.7 ± 1.9 |
| **TS3** | 64.7 ± 3.9 |
| **TS4** | 98.4 ± 6.2 |
| **TS5** | 143.3 ± 9.7 |
| **NC1** | 35.6 ± 2.5 |
| **NC2** | 36.8 ± 1.6 |
| **NC3** | 1.4 ± 0.3 |
| **BM1** | 61.0 ± 1.7 |
| **BM2** | 71.0 ± 2.1 |
| **BM3** | 18.2 ± 0.8 |
| Acarbose (positive control) | 332.5 |

Caffeic acid (NC3). White amorphous powder. $^1$H NMR (500 MHz, Acetone $d_6$) and $^{13}$C NMR (125 MHz, Acetone $d_6$) data were consistent with those reported in the literature (Tošović, 2007) (Fig. S12).

Compounds NC1-3 exhibited strong inhibition of alpha-glucosidase with $IC_{50}$ values of 1.4, 35.6, and 36.8 μM, respectively (Table 2).

### 3.3. Phytochemical identification and alpha-glucosidase inhibition of isolated compounds of Bouea macrophylla

Betullinic acid (BM1), methyl gallate (BM2), and 3-*O*-galloylgallic acid methyl ester (BM3) were isolated from the bioactive HEA extract of *B. macrophylla*.

Betullinic acid (BM1). White amorphous powder. $^1$H NMR (500 MHz, Acetone $d_6$) data were consistent with those reported in the literature (Hossain and Ismail, 2013) (Fig. S13).

Methyl gallate (BM2). White amorphous powder. $^1$H NMR (500 MHz, Acetone $d_6$) data were consistent with those reported in the literature (Kamatham et al., 2015) (Fig. S14).

3-*O*-Galloyl gallic acid methyl ester (BM3). White amorphous powder. $^1$H NMR (500 MHz, Acetone $d_6$) and $^{13}$C NMR (125 MHz, Acetone $d_6$) data were consistent with those reported in the literature (Newsome et al., 2016) (Figs. S15, S16).

Compounds BM1-3 were evaluated the alpha-glucosidase inhibition, showing strong activity with the $IC_{50}$ values of 18.2, 61.0, and 71.0 μM, respectively (see Table 2).

### 3.4. Alpha-glucosidase inhibition type and inhibition constants of BM3

To examine the inhibition mechanism of BM3, activity at pNPG concentrations of 0, 9.3, 18.6, and 37.2 μM was recorded. Lineweaver–Burk plots showed linearity at each concentration, intersecting the y-axis in the first quadrant (Fig. 2).

### 3.5. In silico molecular docking model of compounds NC1, NC2, and BM3

The best conformation ligand NC1, NC2, BM3, and Acarbose (anti-diabetic drug) which had demonstrated low $IC_{50}$ values, were selected for investigation of molecular docking, indicating the consistency between *in vitro* and *in silico* studies of these compounds. The significant results obtained from docking procedure of conformations of ligands, NC1, NC2, and BM3, with the crystal structures of target protein *in silico* molecular docking model were summarized in Table 3.

### 3.6. Molecular dynamics simulation of BM3

The RMSD graph (Fig. 13) illustrated the variations of internal atomic coordinates in the conformations are in the range of

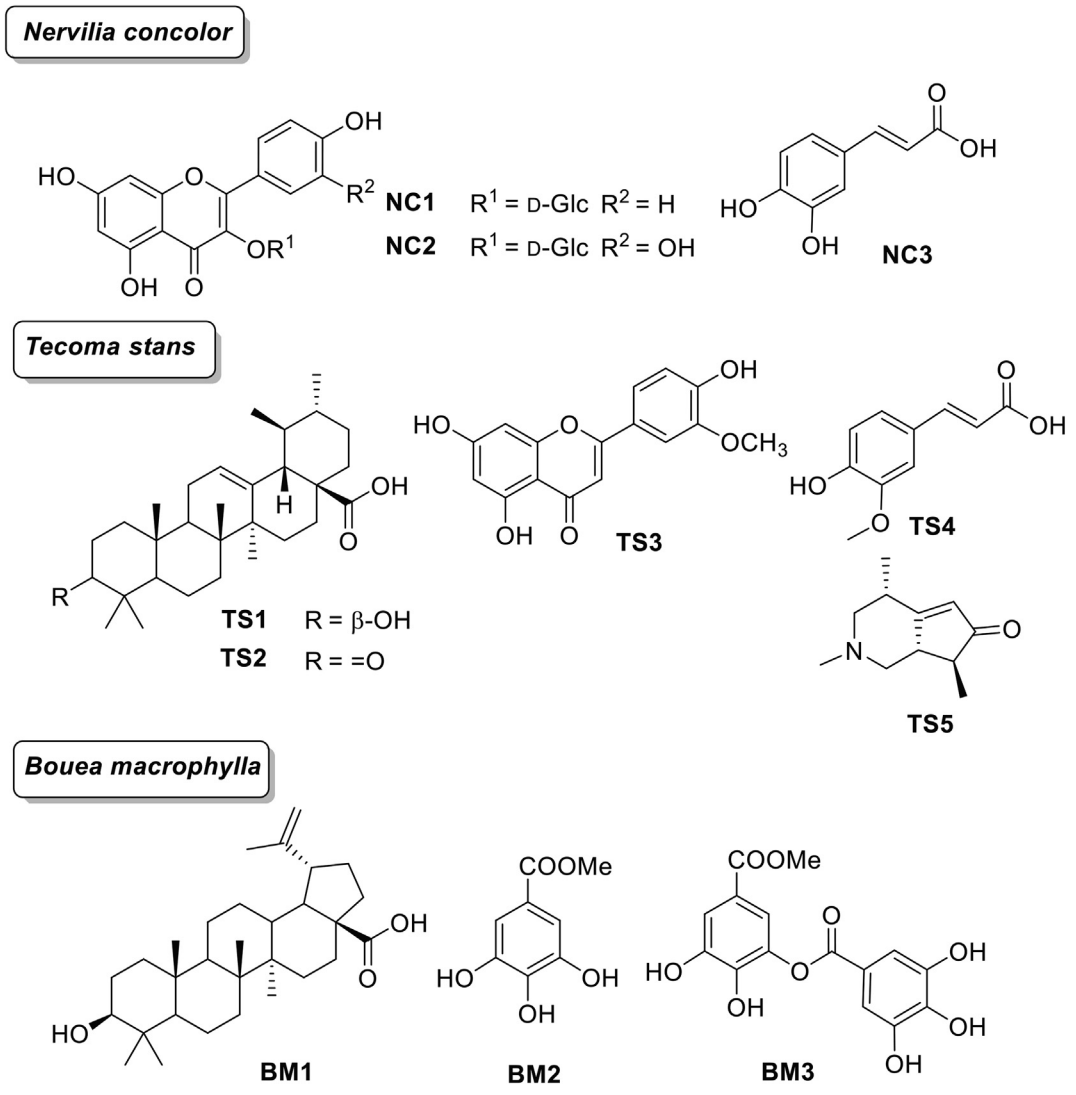


**Fig. 1.** Chemical structures of **NC1-3, TS1-5,** and **BM1-3**.

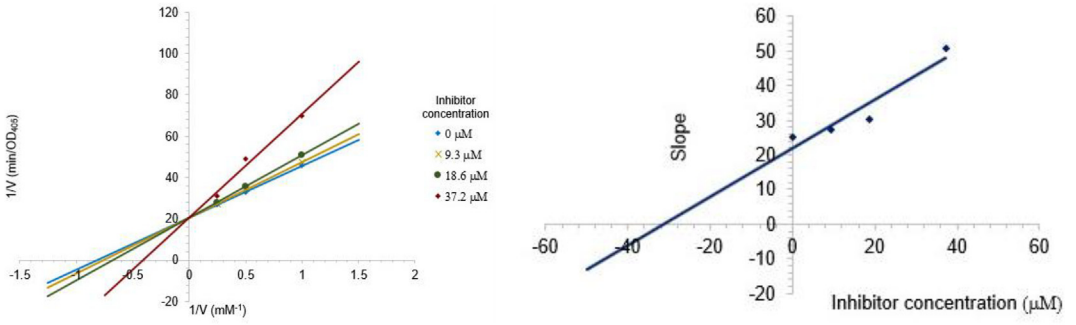


**Fig. 2.** Lineweaver-Burk plot for α-glucosidase inhibition by compound **BM3** (left) and secondary plot of slope vs inhibitor concentration (right).

0.25–0.28 nm and 0.25–0.30 nm for first and second trajectories, respectively, which indicates a system in equilibrium and stability after 30 ns. The RMSD value between MD-refined and original configurations was approximately 0.2 nm being within successful rate of simulation (Al-Shabib et al., 2020). The similarity in the poses of two previously mentioned configurations was illustrated in Fig. 18.

## 4. Discussion

Our literature review showed that crude extracts of *T. stans* have previously been evaluated for alpha-glucosidase inhibition. They include the aqueous extract from *T. stans* leaves, which demonstrated an $EC_{50}$ value of 0.73 mg/mL against intestinal alpha-glucosidase (Aguilar-Santamaría et al., 2009), while the

**Table 3**
Significant results from the *in silico* molecular model of docking and enzyme alpha-glucosidase based on free energy of binding (ΔG), inhibitor constant of fifty percent ($K_i$), number of hydrogen bonds, and the length of hydrogen bonds in units of Å.

| Entry | Free Energy of Binding[a] of the best docking pose | $K_i$[b] | The number of hydrogen bonds[c] | The property and bond length[d] |
|---|---|---|---|---|
| **NC1** | **−7.73 (Pose: 177/200)** | **2.15** | **4** | A:ILE362:N–NC1:O (2.54 Å)<br>NC1:H–A:LEU364:O (1.92 Å)<br>NC1:H–A:ILE362:O (2.18 Å)<br>NC1:H–A:GLN447:O (1.95 Å) |
| **NC2** | **−7.03 (Pose: 106/200)** | **7.08** | **8** | A:GLN447:N–NC2:O (2.96 Å)<br>A:ASN448:N–NC2:O (3.09 Å)<br>A:ASN448:N–NC2:O (3.14 Å)<br>NC2:H– A:ILE362:O (2.08 Å)<br>NC2:H–A:ASP568:O (1.73 Å)<br>NC2:H–A:ASP568:O (2.01 Å)<br>NC2:H–A:PHE444:O (1.94 Å)<br>NC2:H - A:VAL446:O (2.25 Å) |
| **BM3** | **−6.73 (Pose: 134/200)** | **11.72** | **7** | A:ARG428:N–BM3:O (2.64 Å)<br>A:ARG428:N–BM3:O (3.11 Å)<br>BM3:H– A:ILE362:O (2.20 Å)<br>BM3:H– A:ILE362:O (2.34 Å)<br>BM3:H–A:GLN447:O (1.97 Å)<br>BM3:H–A:GLN447:O (1.96)<br>BM3:H–A:GLU429:O (2.09) |
| **Acarbose** | **−6.54 (Pose: 52/200)** | **15.98** | **12** | A:ARG428:N–Acarbose:O (2.84 Å)<br>Acarbose :H–A:VAL446:O (2.28 Å)<br>Acarbose:H–A:VAL446:O (2.36 Å)<br>Acarbose :H–A:GLU443:O (2.28 Å)<br>Acarbose:H–A:GLU443:O (2.26 Å)<br>Acarbose:H–A:GLN445:O (2.01 Å)<br>Acarbose:H–A:GLN442:O (2.18 Å)<br>Acarbose:H–A:GLN442:O (2.01 Å)<br>Acarbose:H - A:LEU364:O (2.20 Å)<br>Acarbose :H - A:GLU443:O (2.06 Å)<br>Acarbose:H–A:GLU443:O (1.95 Å)<br>Acarbose :H–A:ILE362:O (1.82 Å) |

[a]. Calculated using AutoDockTools–1.5.6rc3 and reported in units of kcal.mol$^{-1}$. [b]. Inhibition constants $K_i$, μM derived using AutoDockTools–1.5.6rc3. [c],[d]. Based on Discovery Studio (DSC) software.

methanol and ethyl acetate extracts from the bark showed $IC_{50}$ values of 0.645 mg/mL (Evangeline et al., 2015). However, our study is the first to report alpha-glucosidase inhibition by extracts from *T. stans* flowers. The monoterpene alkaloid tecomine (TS5) is abundant in the leaves and fruits (Marzouk et al., 2006), and has been experimentally demonstrated to produce a significant reduction in the blood sugar of rabbits (Costantino et al., 2003). Rahman et al. (2019) demonstrated that this compound inhibited the alpha-glucosidase enzyme *in silico*. The hydrochloride salt of tecomine (TS5) is known to reduce plasma cholesterol (Costantino et al., 2003). Chrysoeriol (TS3) extracted from *T. stans* leaves shows strong inhibition of the pancreatic lipase enzyme [28]. Ursolic acid (TS1) is known to exhibit strong inhibition of alpha-glucosidase (Wu et al., 2017). The compound 3-oxours-12-en-28-oic acid (TS2) is less potent than TS1, suggesting that the 3-OH group of the ursane skeleton plays a key role in alpha-glucosidase

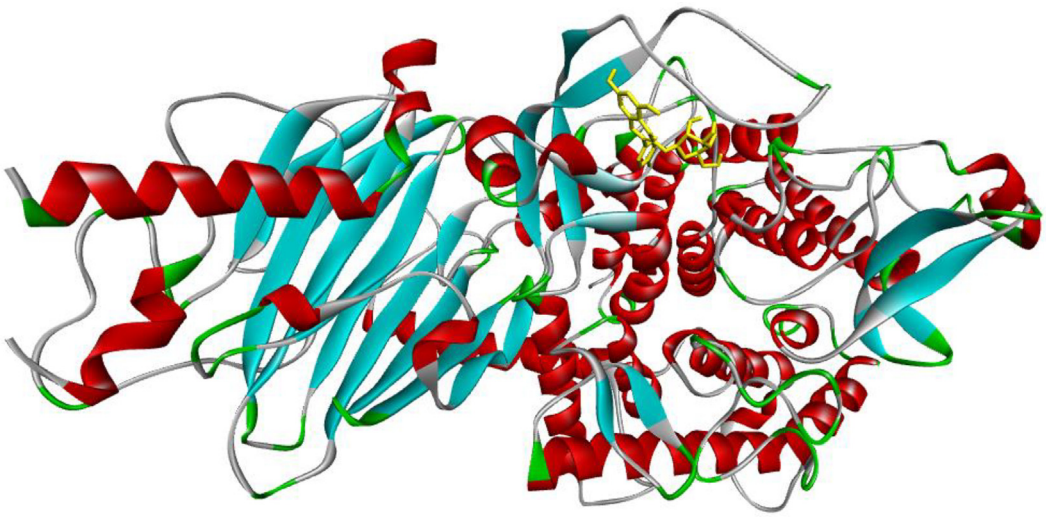

**Fig. 3.** Most stable conformation of ligand **NC1** linked to pocket of the receptor 4J5T. Crystal structure of α-glucosidase enzyme.

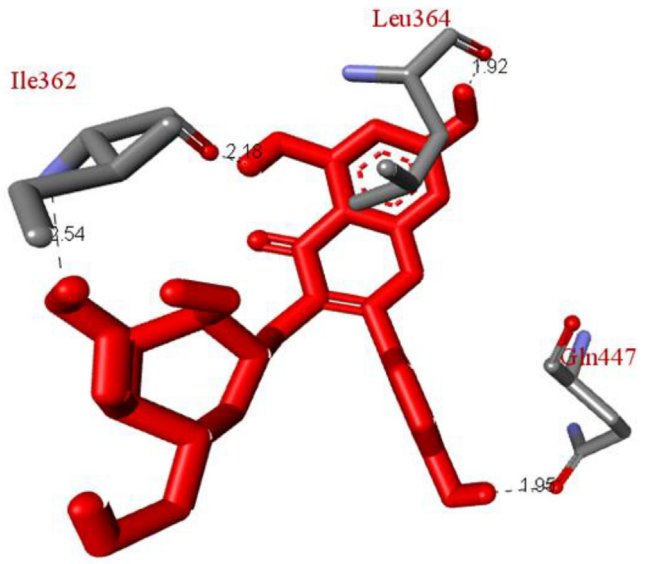


**Fig. 4.** Hydrogen bonds between amino acids of enzyme protein 4J5T and active atoms on conformation ligand **NC1.**

inhibition. Adisakwattana et al. (2009) undertook kinetic studies for caffeic acid (NC3) and ferulic acid (TS4), and concluded that both are non-competitive types.

Astragalin (NC1) and isoquercitrin (NC2) also inhibited alpha-glucosidase, consistent with published results (Hong et al., 2013; Pereira et al. 2011). Caffeic acid (NC3) showed the highest activity, which again was consistent with the literature (Oboh et al., 2015). Adisakwattana et al. (2009) undertook kinetic studies for caffeic acid (NC3) and concluded that both are non-competitive types. A molecular docking model (Damián-Medina et al., 2020) has confirmed the consistency between *in vitro* and *in silico* studies of the two compounds, so no *in silico* or kinetic analysis of caffeic acid (NC3) was performed in the current work.

Gallic acid and its ester, methyl gallate (BM2) are well- known, widely distributed in many higher plants. Betullinic acid is a popular triterpene which could be found as a major compounds deriving from natural sources. Alpha-glucosidase inhibition of these compounds have been investigated extensively. However, little is known about the activity of 3-*O*-galloylgallic acid methyl ester (BM3). Thus, BM3 was used to explore the inhibition mechanism based on its low $IC_{50}$ value among tested compounds.

The *in silico* docking profile of ligand NC1 and alpha-glucosidase enzyme, code 4J5T (protein data bank: PDB), is shown in Figs. 3–6, S1, and Table 3. As can be seen from Fig. 3, in the most stable conformation ligand NC1, docking pose 106/200 (200 models) (brief: ligand) was bound to the pocket on the crystal structure of the glucosidase enzyme 4J5T: PDB with the lowest negative free Gibb energy, $\Delta G^o$, of −7.73 Kcal.mol$^{-1}$ and inhibition constant, Ki, of 2.15 μM. The residual amino acids of A chain the enzyme interacted with active atoms on ligand NC1. As can be seen from Table 3 and Fig. 4, the residual amino acids of the enzyme A chain established four hydrogen bonds with hydrogen, and with the oxygen atoms of the phenolic hydroxy groups of ligand NC1. These were A:ILE362:N–NC1:O, NC1:H–A:LEU364:O, NC1:H–A:ILE362:O, and NC1:H–A:GLN447:O. The NC1:H–A:LEU364:O, hydrogen bond was the strongest, due to the shortest bond length. Fig. 5 shows the main interactions (ligand and residual interactions) as a simple 2D diagram. They included classical hydrogen, pi-sigma, pi-alkyl, Van der Waals forces, and carbon hydrogen bond. In Fig. 5, the most stable ligand NC1 is the capro group (protein identification) via the following ligand interactions: pi-alkyl of Val446 of A chain with the aromatic ring, and the pi-sigma interaction of Leu364 of the A chain with a ring of the conjugation carbonyl with the alkene group, and aromatic ring of ligand NC1. The linker part of ligand NC was not identified, while the functional groups of ligand NC1 linked from Ile362, Leu364, Gln447, and Gly556 of the A chain to hydrogens of the hydroxy phenolic rings or hydroxy benzyl group

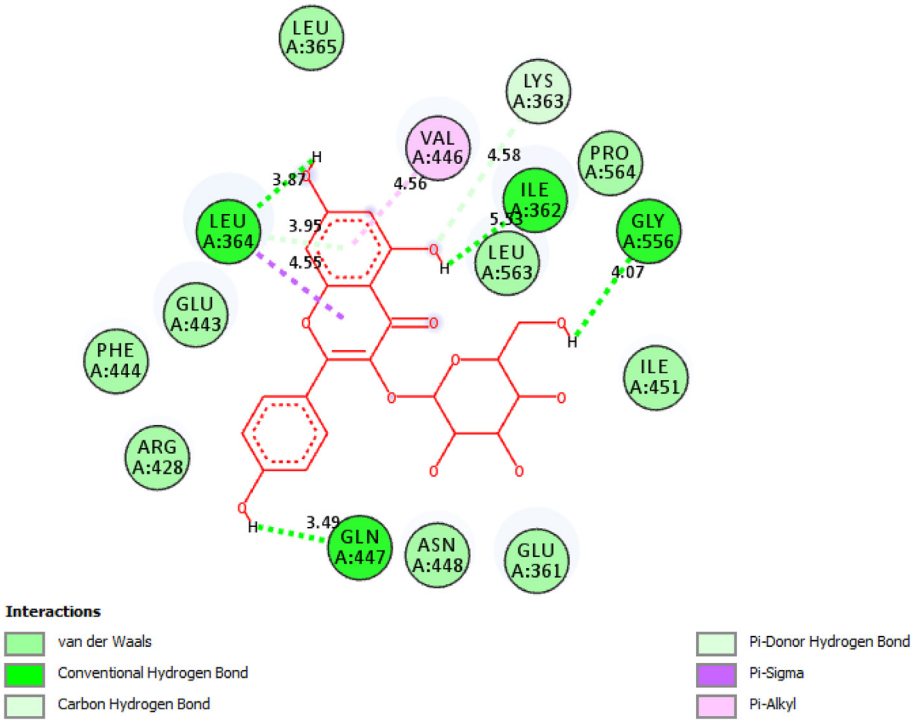


**Fig. 5.** 2D diagram showing important interactions between conformation ligand **NC1** and amino acids of DNA of receptor, 4J5T.

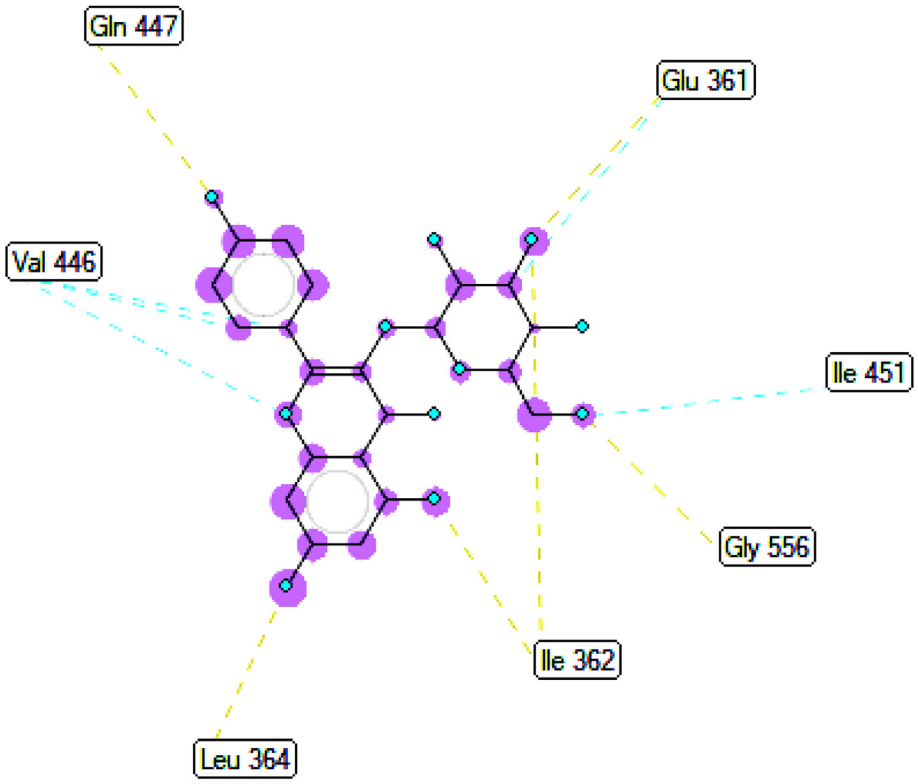


**Fig. 6.** Ligand map showing interactions between **NC1** and 4J5T such as hydrogen bonds (brown lines), steric interactions (light blue lines), and overlap interactions (purple circles).

on ligand NC2. Residual Van der Waals interactions formed from Glu361, Ile361, Lys363, Leu365, Arg428, Glu443, Phe444, Asn448, Leu563, and Pro564 of the A chain of the enzyme pocket with ligand NC1. The ligand NC1 has potential for drug delivery because of the lack of a part of the linker identification. As shown in Fig. 6, the ligand map, secondary interactions formed from active amino acid of A chain to active atoms on ligand NC2 such as hydrogen bonds (from Ile362, Gly556, Glu361, Gln447, and Leu 364 to conformation ligand NC1), steric interactions (from Val446, Glu361, and Ile451 to ligand NC1), and overlap interactions (violet circles). Those interactions determined the strength interactions of ligand NC1 and receptor during docking processing.

Table 3 and Figs S2–S6 show the interaction profile between NC2 and the 4J5T target enzyme. The conformation ligand NC2, docking pose 106/200 binds to enzyme 4J5T with a $\Delta G^{o}$ value of $-7.03$ Kcal.mol$^{-1}$ and Ki value of 7.08 μM, as shown in Table 3.

**Fig. 7.** The ligand **BM3**, the best conformation ligand (color molecule) has bond to active sites on the crystal structure of enzyme α-glucosidase, code: 4J5T: PDB.

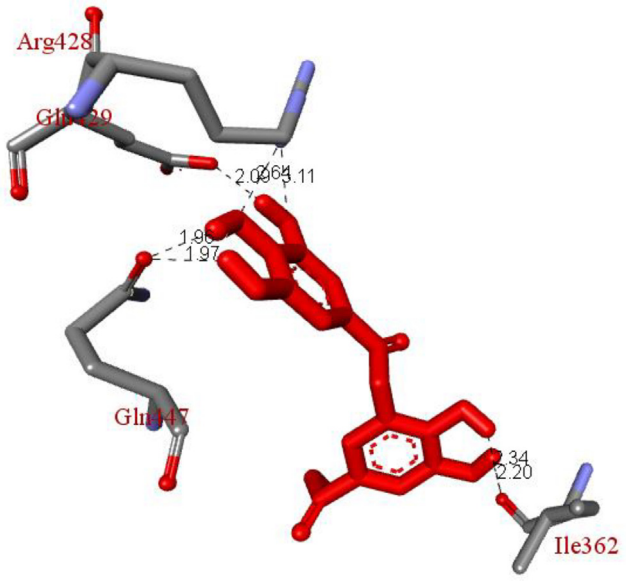


**Fig. 8.** Hydrogen bonds linking residual amino acids to active sites on ligand BM3.

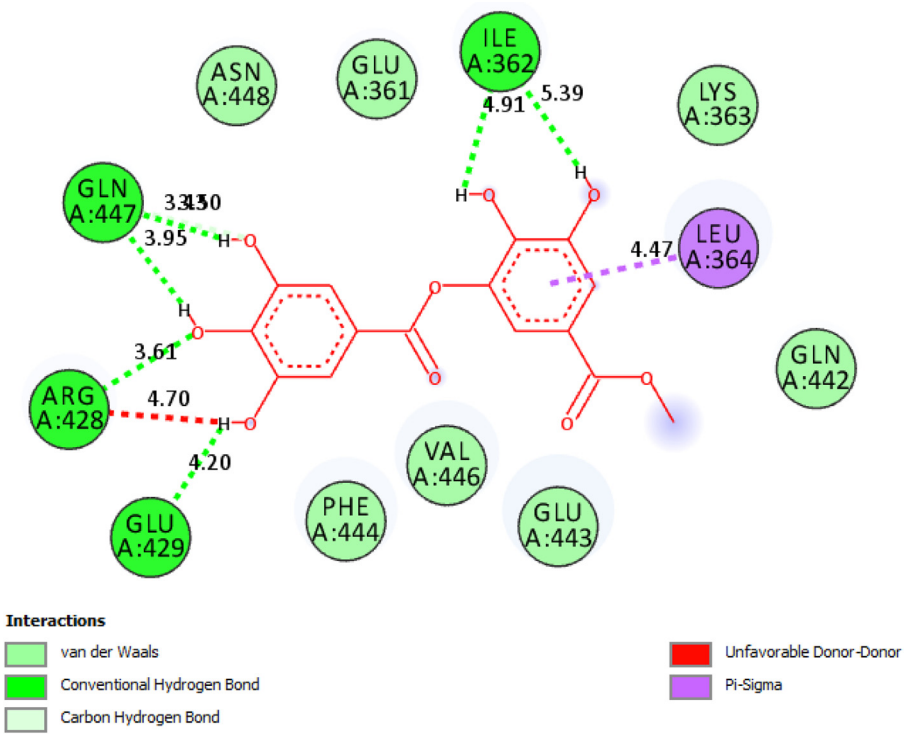


**Fig. 9.** 2D diagram showing major interaction profile of ligand **BM3** and enzyme.

Ligand NC2, pose 106 forms hydrogen bonds with residual amino acids: A:GLN447:N–NC2:O, A:ASN448:N–NC2:O, A:ASN448:N–NC2:O, NC2:H–A:ILE362:O, NC2:H–A:ASP568:O, NC2:H–A:ASP568:O, NC2:H–A:PHE444:O, and NC2:H - A:VAL446:O. Fig. S2 shows conformation ligand NC2 dipping into a pocket of the target enzyme. Ligand NC2 is moderate hydrophilic. The 2D diagram shows the major interactions between ligand NC2 and the target enzyme via hydrogen bonds, pi-sigma, Van der Waals forces, unfavorable donor–donor, and unfavorable acceptor–acceptor in Fig. S3. The ligand binds weakly as the linker of ligand NC2 does not interact with the active amino acids and cap group does not identify much more. In the cap group, part of identification of the protein of the ligand detects interactions including pi-sigma (Leu 563: A to aromatic ring). The functional group of ligand NC2 was identified via the hydrogen bonds from amino acids such as Asp 568, Ile362, Gln447, Phe444, Asn448, and Val446 of the A chain to atom hydrogens and oxygen at hydroxy group of ligand NC2. Residual interactions include weak Van der Waals bonds formed from the amino acids of the enzyme pocket to ligands Glu443, Lys363, Leu364, Arg428, Glu429, and Ile451 of the A chain. The interaction profile of the most stable conformation ligand BM3, docking pose 134/200 is shown in Table 3, Fig. 7–10, and Fig. S7. In Fig. 7, the most stable conformation of ligand BM3, docking pose 134 shows interacting with the active sites of alpha-glucosidase 4J5T: PDB at an enzyme pocket site. In Table 3 and Fig. 8, ligand BM3, docking pose 134 has bound with the target enzyme with a $\Delta G^{o}$ of −6.73 Kcal.mol$^{-1}$ and $K_i$ of 11.72 μM. The docking pose 134 has formed seven hydrogen bonds with residual amino acids such as A:ARG428:N–BM3:O, A:ARG428:N–BM3:O, BM3:H–A:ILE362:O, BM3:H–A:ILE362:O, BM3:H–A:GLN447:O, BM3:H–A:GLN447:O, BM3:H–A:GLU429:O. The BM3:H–A:GLN447:O bond was strongest, having the shortest bond length. The 2D diagram in Fig. 9 shows the main interactions between ligand BM3 (docking pose 134) and the target enzyme. These include the hydrogen bond, pi-sigma, unfavorable donor–donor, carbon hydrogen bond, and Van der Waals interactions. The conformation ligand BM3 (docking pose 134) is a potential drug delivery because it has three parts that recognize the protein of enzyme 4J5T. The protein identification area of ligand BM3 has pi-sigma interaction via Leu 364 of A chain with one aromatic ring. The linker exposes an unfavorable donor–donor interaction of Arg428 of the A chain with an oxygen atom of phenolic hydroxy group of conformation BM3. The functional group identification part of the ligand formed so many hydrogen bonds linking from Arg428 (3.61 Å), Gln447 (3.95 Å), Gln447 (3.43 Å), Ile362 (4.91 Å), Ile362 (5.39 Å), and Glu429 (4.20 Å) to hydro atoms and oxygen atom in the aromatic rings. As shown in Fig. 10, the ligand map shows the secondary

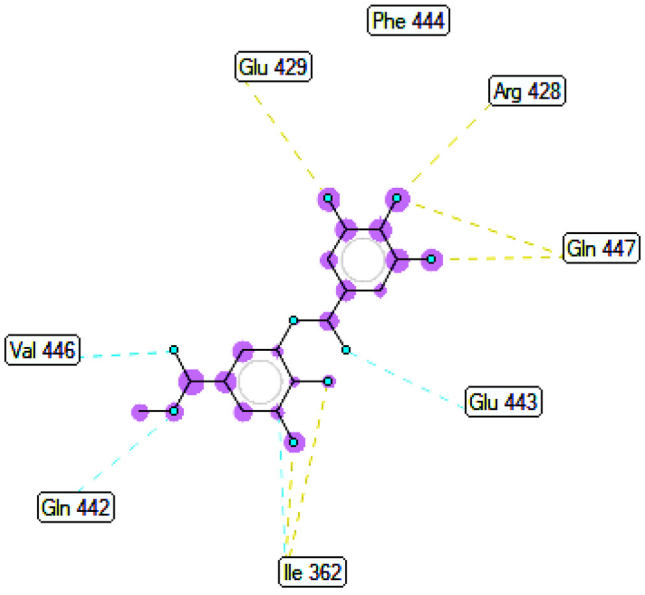


**Fig. 10.** Ligand map from residual amino acids to atoms on ligand BM3.

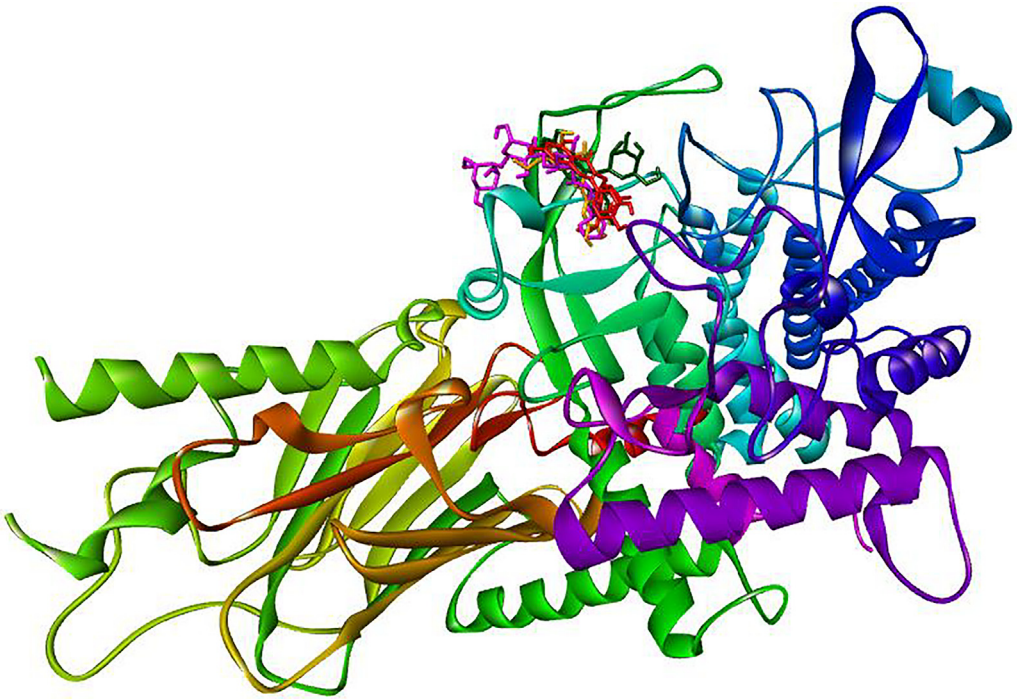

**Fig. 11.** The best docking poses of the most stable conformation ligands have docked to the same active pocket of the crystal structure of enzyme α-glucosidase, 4J5T: PDB. Ligand BM3: the best pose 134 (brown color), ligand NC1: the best pose 177 (dark green color), ligand NC2: the best pose 106 (red color), and ligand Acarbose (standard drug): the best pose 52 (purple color).

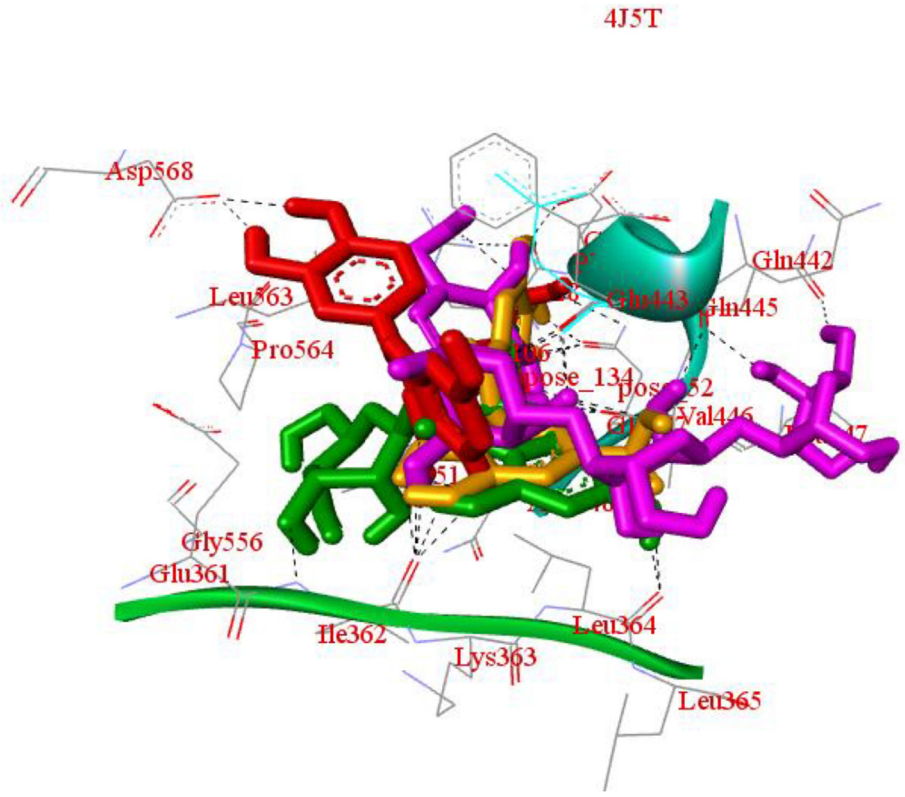


**Fig. 12.** The docking pose of the most conformation ligands, BM3 (pose 134, brown color), NC1 (pose 177, dark green), NC2 (pose 106, red color), and Acarbose (pose 52, purple color) have linked to the same cavity of enzyme, 4J5T.

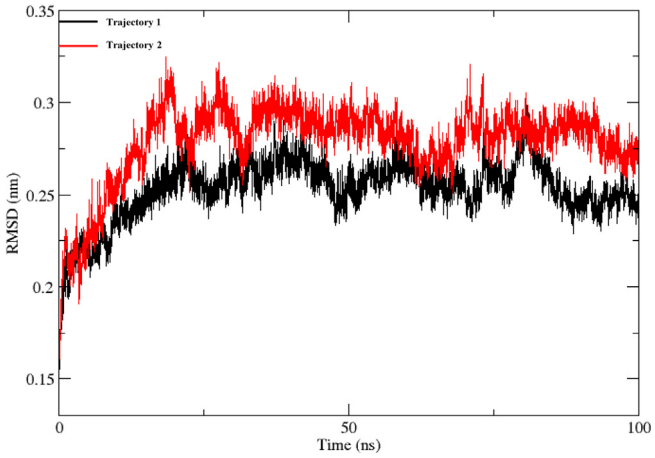


**Fig. 13.** Representational graphic of conformational changes.

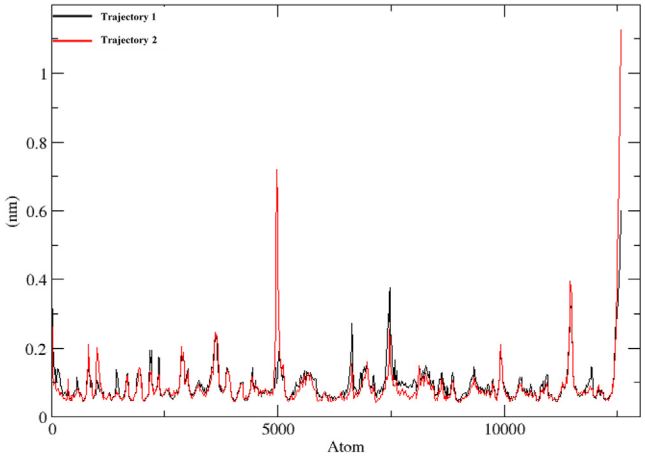


**Fig. 14.** Representational of RMS fluctuations.

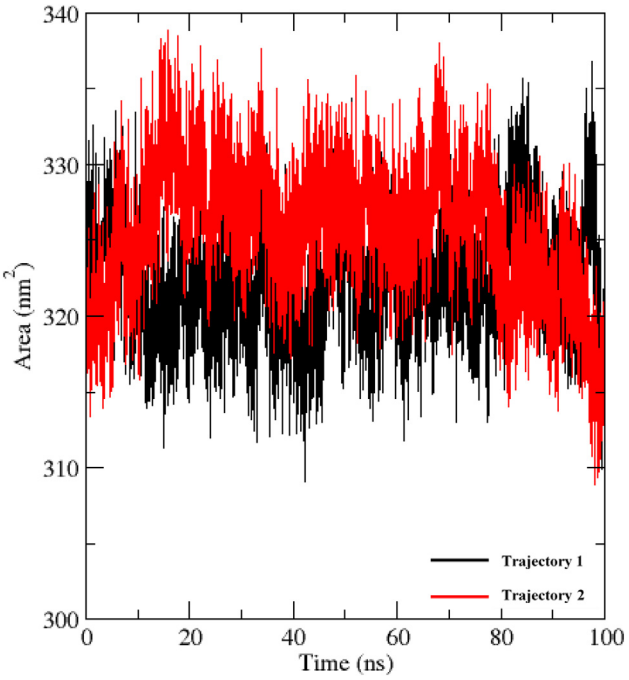


**Fig. 15.** Representational graphic of SASA.

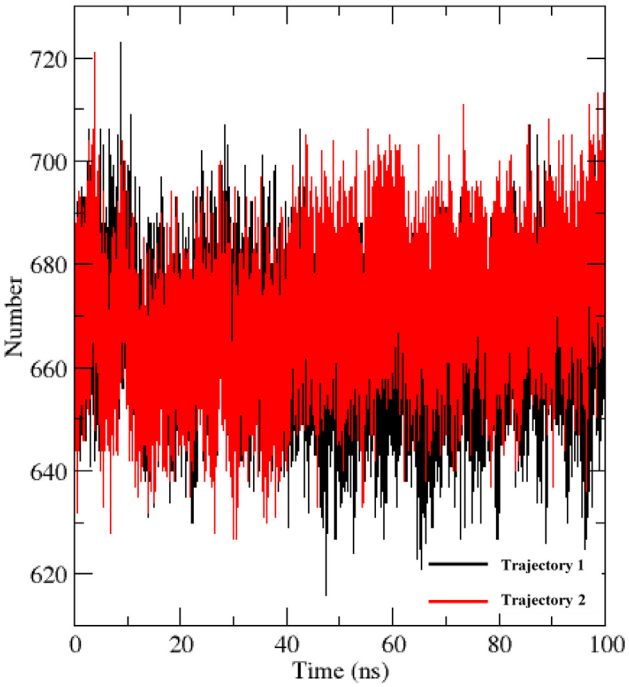


**Fig. 16.** Hydrogen bond numbers.

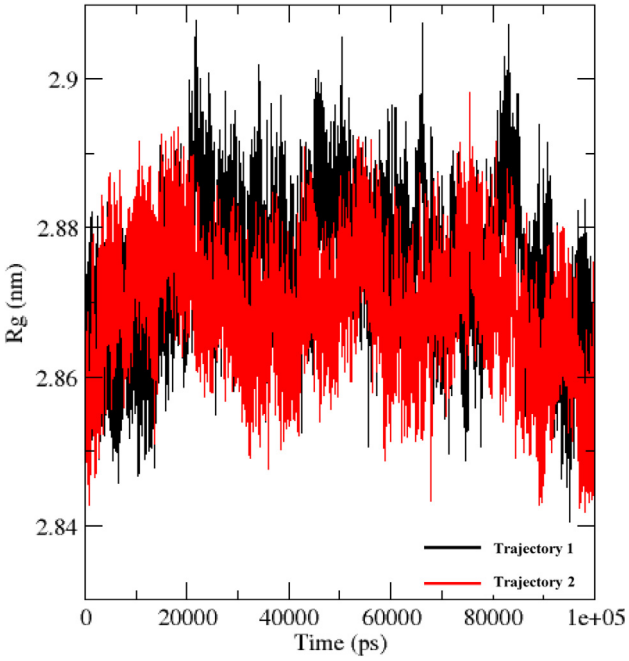


**Fig. 17.** Radius of gyration.

interactions between ligand BM3 and target enzymes via hydrogen bonds (brown lines), steric interactions (light blue lines), and overlap interactions (purple circles). These interactions determine strengths of interactions between ligand BM3 and receptor 4J5T during conformation docking.

The docking of Acarbose (standard drug) to enzyme, 4J5T showed in Fig. S8–S10. The ligand Acarbose (docking pose 52/200) docked to crystal structure of enzyme, 4J5T at active sites of receptor with a $\Delta G^{o}$ value of −6,54 Kcal.mol$^{-1}$ and Ki value of 7.08 μM, as shown in Fig. S8 and Table 3. As can be seen from

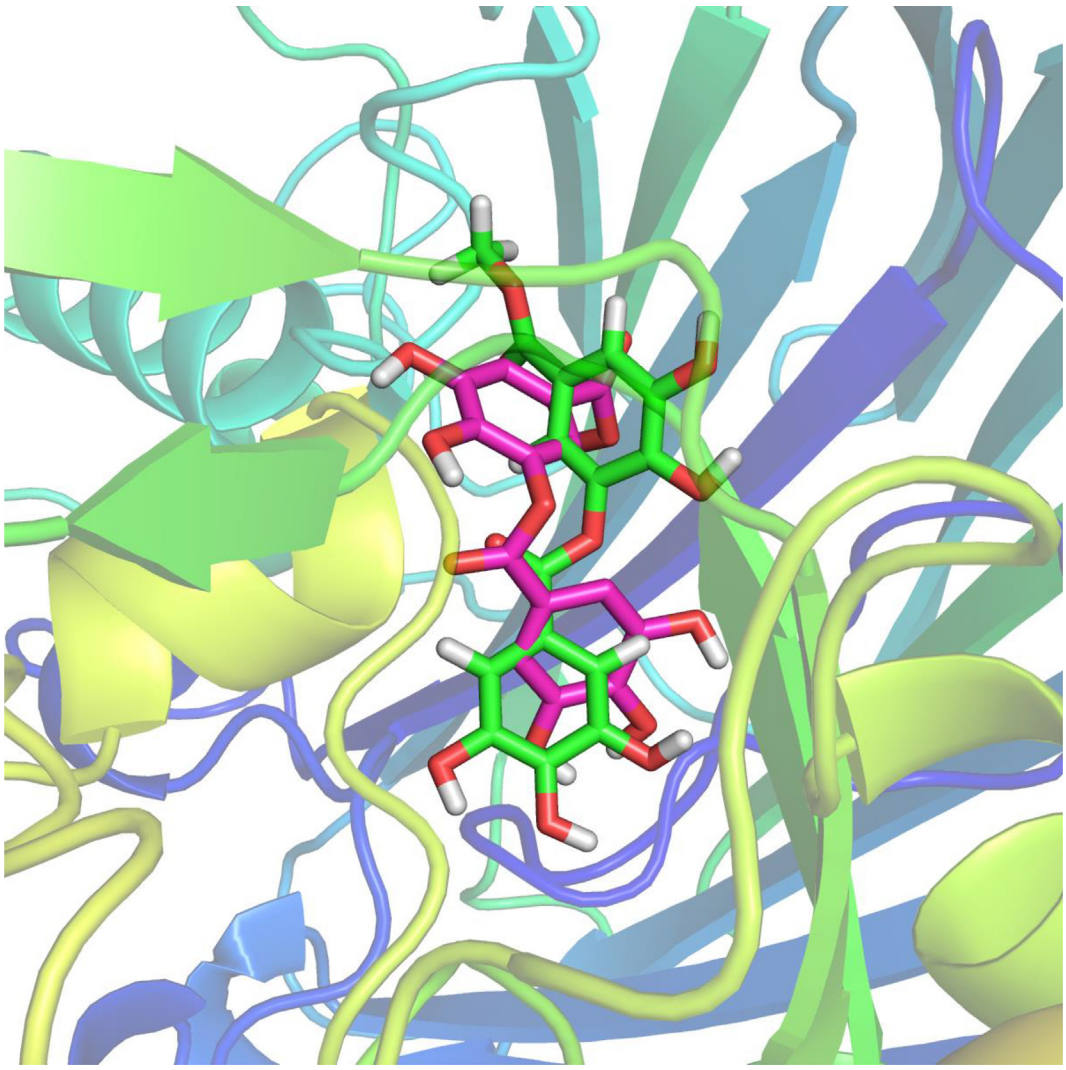

**Fig. 18.** Ligand sites of initial configuration (pink backbone) and MD-refined configuration (green backbone).

**Table 4**
MM/PBSA terms calculated for binding energies.

| | $\Delta E_{elec}$ (kcal/mol) | $\Delta E_{vdW}$ (kcal/mol) | $\Delta G_{polar}$ (kcal/mol) | $\Delta G_{sa}$ (kcal/mol) | $\Delta G_{binding}$ (kcal/mol) |
|---|---|---|---|---|---|
| Trajectory 1 | −50.61 | −51.05 | 70.81 | −5.52 | −36.37 |
| Trajectory 2 | −50.61 | −51.05 | 70.81 | −5.52 | −36.37 |

Table 3 and Fig. S9, the residual amino acids of the enzyme A chain established twelve hydrogen bonds from them to hydro atoms and oxygen on hydroxy groups of ligand Acarbose. They were A:ARG428:N–Acarbose:O, Acarbose:H–A:VAL446:O, Acarbose:H–A:VAL446:O, Acarbose :H–A:GLU443:O, Acarbose:H–A:GLU443:O, Acarbose:H–A:GLN445:O, Acarbose:H–A:GLN442:O, Acarbose:H–A:GLN442:O, Acarbose:H–A:LEU364:O, Acarbose :H–A:GLU443:O, Acarbose:H–A:GLU443:O, and Acarbose :H–A:ILE362:O (1.82 Å) as shown in Table 3 and Fig. S9. As can be seen from Fig. S10, ligand Acarbose was fully identified as good drug deliver because three parts of ligand find out well. The cap group linked from Glu443 to the heterocyclic oxygen (via an unfavorable acceptor–acceptor interaction), the linker bound from Phe444 to oxygen atom of method group (via an unfavorable acceptor–acceptor interaction). The functional groups obtained via hydrogen bonds from Arg428, Ile362, Glu443, Val446, Leu364, Gln442, and Gln445 to hydro atoms, oxygen atom on ligand Acarbose. The ligand BM3 docked to enzyme, 4J5T better than that of ligand Acarbose because those values of free Gibbs energy and inhibition constant of ligand BM3 (docking pose 134) were lower than those of ligand Acarbose (docking pose 52).

In *silico* docking model, the redocking has been made to prove the validation of this docking. As shown in Fig. 11, the best stable conformation docking of ligand such as BM3 (pose 134, brown color), NC1 (pose 177, dark green color), NC2 (pose106, red color), and Acarbose (standard drug) docked to the same active pocket of the crystal structure of enzyme α-glucosidase, 4J5T: PDB, respectively. As seen in Fig. 12, those docking poses of the ligand BM3, NC1, NC2, and Acarbose docked to the same cavity of receptor 4J5T. Their structures are not superimposed because they are not analog structures or conformation isomers. They mean docking poses, which docked to the same cavity, when it was compared to one stand drug, Acarbose as reference.

The analysis of RMSF, $R_g$, SASA, hydrogen bond numbers (Figs. 14–17) and MM/PBSA energies (Table 4) also show a highly similarity in these two simulated trajectories. The MM/PBSA

binding energies based on two MD trajectories shown in Table 1 are remarkably identical, at approximately −36.37 kJ/mol. Due to the considerably lengthy computational time required, the entropic term of the binding energy was overlooked in the calculations in MM/PBSA method. However, if only the terms of $\Delta G_{binding}$ calculated by MM/PBSA, docking, and $IC_{50}$ value were considered, it is suggested that later study should explored the entropic terms for more comprehensive energy estimations. In this study, the docking method has been illustrated as faster, reliable, and applicable for rapidly determining the binding energies as well as modeling the spatial poses of ligand – alpha-glucosidase complexes with acceptable accuracy.

The kinetics of enzyme inhibition confirmed that BM3 acted as a competitive inhibitor. The kinetic analysis showed that an increase in the BM3 concentration had no effect on the Vmax (0.049 μM.min$^{-1}$), but increased the Km from 1.24 to 2.58. The inhibition constant (Ki) was 31.22 μM.

## 5. Conclusions

The non-aqueous extracts of *N. concolor, T. stans,* and *B. macrophylla* showed strong alpha-glucosidase inhibition, guiding bioactive isolation. Eleven compounds were isolated from these three plants, and were elucidated as ursolic acid (TS1), 3-oxours-12-en-28-oic acid (TS2), chrysoeriol (TS3), ferulic acid (TS4), ecomine (TS5), astragalin (NC1), isoquercitrin (NC2), caffeic acid (NC3), betullinic acid (BM1), methyl gallate (BM2), and 3-*O*-galloyl gallic acid methyl ester (BM3). All compounds showed good alpha-glucosidase inhibition, with $IC_{50}$ values ranging from 1.4 to 143.3 μM, indicating that those compounds might account for the activity of the extracts. Among the compounds isolated, NC1-3 and BM3 showed the strongest activity. The kinetics of enzyme inhibition showed that BM3 was a competitive-type inhibitor of alpha-glucosidase. An *in silico* molecular docking model indicated that compounds NC1, NC2, and BM3 were inhibitors of the alpha-glucosidase enzyme. The simulation of the molecular dynamics was performed for compound BM3 and emphasized both the affinity and stability of the ligand with the protein during contacting in the 100 ns time period.

## Declaration of Competing Interest

The authors declare that they have no known competing financial interests or personal relationships that could have appeared to influence the work reported in this paper.

## Appendix A. Supplementary material

Supplementary data to this article can be found online at https://doi.org/10.1016/j.sjbs.2021.09.070.

## References


Al-Shabib, N.A., Khan, J.M., Malik, A., Tabish Rehman, M., AlAjmi, M.F., Husain, F.M., Hisamuddin, M., Altwaijry, N., 2020. Molecular interaction of tea catechin with bovine β-lactoglobulin: A spectroscopic and in silico studies. Saudi Pharmaceut. J. 28 (3), 238–245. https://doi.org/10.1016/j.jsps.2020.01.002.

Anand, M., Basavaraju, R., 2020. A review on phytochemistry and pharmacological uses of *Tecoma stans* (L.). Juss. ex Kunth. J. Ethnopharmacol. 265, 113270. https://doi.org/10.1016/j.jep.2020.113270.

Adisakwattana, S., Chantarasinlapin, P., Thammarat, H., Yibchok-Anun, S., 2009. A series of cinnamic acid derivatives and their inhibitory activity on intestinal α-glucosidase. J. Enzyme Inhib. Med. Chem 24 (5), 1194–1200. https://doi.org/10.1080/14756360902779326.

Aguilar-Santamaría, L., Ramírez, G., Nicasio, P., Alegría-Reyes, C., Herrera-Arellano, A., 2009. Antidiabetic activities of *Tecoma stans* (L.). Juss. ex Kunth. J. Ethnopharmacol. 124 (2), 284–288. https://doi.org/10.1016/j.jep.2009.04.033.

Basir, D., Julinar, J., Agustriana, E., Untari, B., 2014. Oxidation and acetylation of ursolic and oleanolic acids isolated from Fragraea fragrans fruits; antiproliferation of P388 Leukemia Cells. Indones. J. Chem. 14 (3), 269–276. https://doi.org/10.22146/ijc.21238.

Bashyal, P., Parajuli, P., Pandey, R.P., Sohng, J.K., 2019. Microbial biosynthesis of antibacterial chrysoeriol in recombinant *Escherichia coli* and bioactivity assessment. Catalysts 9 (2), 112. https://doi.org/10.3390/catal9020112.

Costantino, L., Raimondi, L., Pirisino, R., Brunetti, T., Pessotto, P., Giannessi, F., Lins, A.P., Barlocco, D., Antolini, L., El-Abady, S.A., 2003. Isolation and pharmacological activities of the *Tecoma stans* alkaloids. Il Farmaco 58 (9), 781–785. https://doi.org/10.1016/S0014-827X(03)00133-2.

Chen, J.-M., Wei, L.-B., Lu, C.-L., Zhou, G.-X., 2013. A flavonoid 8-C-glycoside and a triterpenoid cinnamate from *Nervilia fordii*. J. Asian Nat. Prod. Res. 15 (10), 1088–1093. https://doi.org/10.1080/10286020.2013.814107.

Damián-Medina, K., Salinas-Moreno, Y., Milenkovic, D., Figueroa-Yáñez, L., Marino-Marmolejo, E., Higuera-Ciapara, I., Vallejo-Cardona, A., Lugo-Cervantes, E., 2020. *In silico* analysis of antidiabetic potential of phenolic compounds from blue corn (*Zea mays L.*) and black bean (*Phaseolus vulgaris L.*). Heliyon 6 (3), e03632. https://doi.org/10.1016/j.heliyon.2020.e03632.

Dechsupa, N., Kantapan, J., Tungjai, M., Intorasoot, S., 2019. Maprang "*Bouea macrophylla* Griffith" seeds: proximate composition, HPLC fingerprint, and antioxidation, anticancer and antimicrobial properties of ethanolic seed extracts. Heliyon 5 (7), e02052. https://doi.org/10.1016/j.heliyon.2019.e02052.

Devi, A.P., Duong, T.-H., Ferron, S., Beniddir, M.A., Dinh, M.-H., Nguyen, V.-K., Pham, N.-K.-T., Mac, D.-H., Boustie, J., Chavasiri, W., Pogam, P.L., 2020. Salazinic acid-derived depsidones and diphenylethers with α-glucosidase inhibitory activity from the lichen *Parmotrema dilatatum*. Planta Med. 86 (16), 1216–1224. https://doi.org/10.1055/a-1203-0623.

Dohnal, B., 1977. Investigations on some metabolites of *Tecoma stans* Juss. callus tissue. Part III. Chromatographical search for iridoids, phenolic acids, terpenoids and sugars. Acta Soc. Bot. Pol. 46 (2), 187–199. https://doi.org/10.5586/asbp.1977.015.

Duong, T.-H., Paramita Devi, A., Tran, N.-M.-A., Phan, H.-V.-T., Huynh, N.-V., Sichaem, J., Tran, H.-D., Alam, M., Nguyen, T.-P., Nguyen, H.-H., Chavasiri, W., Nguyen, T.-C., 2020. Synthesis, α-glucosidase inhibition, and molecular docking studies of novel N-substituted hydrazide derivatives of atranorin as antidiabetic agents. Bioorg. Med. Chem. Lett. 30 (17), 127359. https://doi.org/10.1016/j.bmcl.2020.127359.

Evangeline, R.M., Murugan, N., Kumar, P.P., Christhudas, I.N., 2015. *In vitro* studies on α-glucosidase inhibition, antioxidant and free radical scavenging properties of *Tecoma stans*. Int. J. Pharm. Pharmaceut. Sci. 7, 44–49 https://www.researchgate.net/publication/281654058.

Fitri, L., Taufiqurrahman, I., Irnamanda, D.H., 2018. Phytochemical and cytotoxicity testing of ramania leaves (*Bouea macrophylla* Griffith) ethanol extract toward vero cells using mtt assay method (Preliminary study of adjuvant therapy materials to the preparation of the drug). Dentino 3 (1), 51–56. https://doi.org/10.20527/dentino.v3i1.4617.

Gale, S., Yukawa, T., Kuroiwa, N., 2007. Studies in Asian Nervilia (Orchidaceae) I: Neotypification and circumscription of *N. nipponica* in Japan. Kew Bull. 62, 85–94 https://www.jstor.org/stable/20443317.

Jorgensen, W.L., Chandrasekhar, J., Madura, J.D., Impey, R.W., Klein, M.L., 1983. Comparison of simple potential functions for simulating liquid water. J. Chem. Phys. 79 (2), 926–935. https://doi.org/10.1063/1.445869.

Kamatham, S., Kumar, N., Gudipalli, P., 2015. Isolation and characterization of gallic acid and methyl gallate from the seed coats of Givotia rottleriformis Griff. and their anti-proliferative effect on human epidermoid carcinoma A431 cells. Toxicol. Rep. 2, 520–529. https://doi.org/10.1016/j.toxrep.2015.03.001.

Kumar, K.G., Boopathi, T., 2018. An updated overview on pharmacognostical and pharmacological screening of *Tecoma stans*. PharmaTutor 6 (1), 38–49. https://doi.org/10.29161/PT.v6.i1.2017.38.

Kameshwara, S., Kothai, A.R., Jothimaniv, C., Senthilkum, R., 2013. Evaluation of hepatoprotective activity of *Tecoma stans*. Flowers. Pharmacologia. 4 (3), 236–242. https://doi.org/10.5567/pharmacologia.2013.236.242.

Hong, H.C., Li, S.L., Zhang, X.Q., Ye, W.C., Zhang, Q.W., 2013. Flavonoids with α-glucosidase inhibitory activities and their contents in the leaves of *Morus atropurpurea*. Chin. Med. 8 (1), 1–7. https://doi.org/10.1186/1749-8546-8-19.

Hossain, M.A., Ismail, Z., 2013. Isolation and characterization of triterpenes from the leaves of *Orthosiphon stamineus*. Arab. J. Chem. 6 (3), 295–298. https://doi.org/10.1016/j.arabjc.2010.10.009.

Lindorff-Larsen, K., Piana, S., Palmo, K., Maragakis, P., Klepeis, J.L., Dror, R.O., Shaw, D.E., 2010. Improved side-chain torsion potentials for the Amber ff99SB protein force field. Proteins 78 (8), 1950–1958. https://doi.org/10.1002/prot.22711.

Lins, A.P., Felicio, J.D., 1993. Monoterpene alkaloids from *Tecoma stans*. Phytochemistry 34 (3), 876–878. https://doi.org/10.1016/0031-9422(93)85381-Z.

Marzouk, M.S., Gamal-Eldeen, A.M., Mohamed, M.A., El-Sayed, M.M., 2006. Antioxidant, and anti-proliferative active constituents of *Tecoma stans* against tumor cell lines. Nat. Prod. Commun. 1 (9), 735–743. https://doi.org/10.1177/1934578X0600100908.

Napolitano, J.G., Lankin, D.C., Chen, S.-N., Pauli, G.F., 2012. Complete 1H NMR spectral analysis of ten chemical markers of *Ginkgo biloba*. Magn. Reson. Chem. 50 (8), 569–575. https://doi.org/10.1002/mrc.v50.810.1002/mrc.3829.

Ngo, S.T., Tam, N.M., Pham, M.Q., Nguyen, T.H., 2021. Benchmark of Popular Free Energy Approaches Revealing the Inhibitors Binding to SARS-CoV-2 Mpro. J. Chem. Inf. Model. 61 (5), 2302–2312. https://doi.org/10.1021/acs.jcim.1c00159.

Nguyen, N.H., Nguyen, T.T., Ma, P.C., Ta, Q.T.H., Duong, T.H., Vo, V.G., 2020. Potential antimicrobial and anticancer activities of an ethanol extract from *Bouea*

*macrophylla*. Molecules 25 (8), 1996. https://doi.org/10.3390/molecules25081996.
Newsome, A.G., Li, Y., van Breemen, R.B., 2016. Improved quantification of free and ester-bound gallic acid in foods and beverages by UHPLC-MS/MS. J. Agric. Food Chem. 64 (6), 1326–1334. https://doi.org/10.1021/acs.jafc.5b04966.
Oboh, G., Agunloye, O.M., Adefegha, S.A., Akinyemi, A.J., Ademiluyi, A.O., 2015. Caffeic and chlorogenic acids inhibit key enzymes linked to type 2 diabetes (in vitro): a comparative study. J. Basic Clin. Physiol. Pharmacol. 26 (2), 165–170. https://doi.org/10.1515/jbcpp-2013-0141.
Pereira, D.F., Cazarolli, L.H., Lavado, C., Mengatto, V., Figueiredo, M.S.R.B., Guedes, A., Pizzolatti, M.C., Silva, F.R.M.B., 2011. Effects of flavonoids on α-glucosidase activity: potential targets for glucose homeostasis. Nutr. 27 (11–12), 1161–1167. https://doi.org/10.1016/j.nut.2011.01.008.
Poli, G., Granchi, C., Rizzolio, F., Tuccinardi, T., 2020. Application of MM-PBSA Methods in Virtual Screening. Molecules 25, 1971–1990. https://doi.org/10.3390/molecules25081971.
Qiu, L.i., Jiao, Y., Xie, J.-Z., Huang, G.-K., Qiu, S.-L., Miao, J.-H., Yao, X.-S., 2013. Five new flavonoid glycosides from *Nervilia fordii*. J. Asian. Nat. Prod. Res. 15 (6), 589–599. https://doi.org/10.1080/10286020.2013.790377.
Rahman, N., Muhammad, I., Khan, H., Aschner, M., Filosa, R., Daglia, M., 2019. Molecular docking of isolated alkaloids for possible α-glucosidase inhibition. Biomolecules 9 (10), 544. https://doi.org/10.3390/biom9100544.
Rajan, N.S., Bhat, R., 2016. Antioxidant compounds and antioxidant activities in unripe and ripe kundang fruits (*Bouea macrophylla* Griffith). Fruits 71 (1), 41–47. https://doi.org/10.1051/fruits/2015046.
Raju, S., Kavimani, S., Uma, M.R.V., Sreeramulu, R.K., 2011a. *Tecoma stans* (L.) Juss. ex Kunth (Bignoniaceae): Ethnobotany, phytochemistry and pharmacology. J. Pharm Biomed. Sci. 8 (7), 1–5.
Raju, S., Kavimani, S., Uma Maheshwara rao, V., Sreeramulu Reddy, K., Vasanth Kumar, G., 2011b. Floral extract of *Tecoma stans*: a potent inhibitor of gentamicin-induced nephrotoxicity in vivo. Asian Pac. J. trop. Med. 4 (9), 680–685. https://doi.org/10.1016/S1995-7645(11)60173-9.
Rezende, F.M., Ferreira, M.J.P., Clausen, M.H., Rossi, M., Furlan, C.M., 2019. Acylated flavonoid glycosides are the main pigments that determine the flower colour of the Brazilian native tree *Tibouchina pulchra* (Cham.). Cogn. Molecules 24 (4), 718. https://doi.org/10.3390/molecules24040718.
Shimomura, H., Sashida, Y., Mimaki, Y., Kudo, Y., Maeda, K., 1988. New phenylpropanoid glycerol glucosides from the bulbs of *Lilium* species. Chem. Pharm. Bull. 36 (12), 4841–4848. https://doi.org/10.1248/cpb.36.4841.
Sibanyoni, M.N., Chaudhary, S.K., Chen, W., Adhami, H.-R., Combrinck, S., Maharaj, V., Schuster, D., Viljoen, A., 2020. Isolation, in vitro evaluation, and molecular docking of acetylcholinesterase inhibitors from South African Amaryllidaceae. Fitoterapia 146, 104650. https://doi.org/10.1016/j.fitote.2020.104650.
Sousa da Silva, A.W., Vranken, W.F., 2012. ACPYPE-AnteChamber PYthon Parser interfacE. BMC Res. Notes 5, 367–371. https://doi.org/10.1186/1756-0500-5-367.
Sukalingam, K., 2018. Preliminary phytochemical analysis and *in vitro* antioxidant properties of Malaysian 'Kundang' (*Bouea macrophylla* Griffith). Trends Phytochem. Res. 2 (4), 261–266 http://tpr.iau-shahrood.ac.ir/article_544923.html.
Taher, M.A.H., Dawood, D.H., Sanad, M.I., Hassan, R.A., 2016. Searching for anti-hyperglycemic phytomolecules of *Tecoma stans*. Eur. J. Chem. 7 (4), 397–404. https://doi.org/10.5155/eurjchem.7.4.397-404.1478.
Tian, L.-W., Pei, Y., Zhang, Y.-J., Wang, Y.-F., Yang, C.-R., 2009. 7-O-methylkaempferol and quercetin glycosides from the whole plant of *Nervilia fordii*. J. Nat. Prod. 72 (6), 1057–1060. https://doi.org/10.1021/np800760p.
Tran, T.N.M., Bernadat, G., Mai, D.T., Nguyen, V.K., Sichaem, J., Nguyen, T.P., Tran, C. L., Do, P.V., Tran, N.M.A., Nguyen, H.H., Beniddir, M.A., Duong, T.H., Le Pogam, P., 2019a. Nervisides I-J: unconventional side-chain-bearing cycloartane glycosides from *Nervilia concolor*. Molecules 24, 2599–2607. https://doi.org/10.3390/molecules24142599.
Tran, T.N.M., Do, P.V., Nguyen, T.P., Phan, N.M., Mai, D.T., Tran, N.M.A., Duong, T.H., Tran, C.L., 2019b. Four flavonols form the whole plant of *Nervilia aragoana*. Vietnam J. Chem. 57 (3), 375–378. https://doi.org/10.1002/vjch.201900047.
Tran, C.L., Dao, T.B.N., Tran, T.N., Mai, D.T., Tran, T.M.D., Tran, N.M.A., Dang, V.S., Vo, T.X., Duong, T.H., Sichaem, J., 2021. Alpha-glucosidase inhibitory diterpenes from *Euphorbia antiquorum* growing in Vietnam. Molecules 26, 2257. https://doi.org/10.3390/molecules26082257.
Tošović, J., 2007. Spectroscopic features of caffeic acid: theoretical study. Kragujevac J. Sci. 39, 99–108. https://doi.org/10.5937/KgJSci1739099T.
Thummajitsakul, S., Silprasit, K., 2017. Genetic differentiation and antioxidant activities of *Bouea macrophylla* Griffith in Nakhon Nayok province. J. Appl. Biol. Chem. 60 (1), 41–47. https://doi.org/10.3839/jabc.2017.008.
Wu, P.P., Zhang, B.J., Cui, X.P., Yang, Y., Jiang, Z.Y., Zhou, Z.H., Zhong, Y.Y., Mai, Y.Y., Ouyang, Z., Chen, H.S., Zheng, J., Zhao, S.Q., Zhang, K., 2017. Synthesis and biological evaluation of novel ursolic acid analogues as potential α-glucosidase inhibitors. Sci. rep. 7 (1), 1–12. https://doi.org/10.1038/srep45578.
Zhou, G.-X., Lu, C.-L., Wang, H.-S., Yao, X.-S., 2009. An acetyl flavonol from *Nervilia fordii* (Hance) Schltr. J. Asian Nat. Prod. Res. 11 (6), 498–502. https://doi.org/10.1080/10286020902893074.
Zhang, L., Zhao, Z.X., Lin, C.Z., Zhu, C.C., Gao, L., 2012. Three new flavonol glycosides from *Nervilia fordii*. Phytochem. Lett. 5, 104–107. https://doi.org/10.1016/j.phytol.2011.11.003.

## Further Reading

Da Silva, A.W.S., Vranken, W.F., 2012. ACPYPE-Antechamber python parser interface. BMC Res. Notes 5 (1), 367. https://doi.org/10.1186/1756-0500-5-367.
Ramirez, G., Zamilpa, A., Zavala, M., Perez, J., Morales, D., Tortoriello, J., 2016. Chrysoeriol and other polyphenols from *Tecoma stans* with lipase inhibitory activity. J. Ethnopharmacol. 185, 1–8. https://doi.org/10.1016/j.jep.2016.03.014.